2D Materials

Printable and flexible graphene pH sensors utilising thin film melanin for physiological applications

2D Materials

OPEN ACCESS

RECEIVED
20 October 2019

REVISED
15 January 2020

ACCEPTED FOR PUBLICATION
4 February 2020

PUBLISHED
28 February 2020

PAPER

Printable and flexible graphene pH sensors utilising thin film melanin for physiological applications

Z Tehrani[1,5], S P Whelan[1,5], A B Mostert[2], J V Paulin[3], M M Ali[1], E Daghigh Ahmadi[1], C F O Graeff[4], O J Guy[2] and D T Gethin[5]

[1] Centre for Nano Health, College of Engineering, Swansea University, Swansea SA2 8PP, United Kingdom
[2] Department of Chemistry, College of Science, Swansea University, Swansea SA2 8PP, United Kingdom
[3] Post-Graduate Program in Materials Science and Technology, São Paulo State University (UNESP), Bauru, Brazil
[4] Department of Physics, São Paulo State University (UNESP), School of Sciences, Bauru, Brazil
[5] Welsh Centre for Printing and Coating, College of Engineering, Swansea University, Swansea SA1 8EN, United Kingdom

E-mail: Z.Tehrani@swansea.ac.uk **and** D.T.Gethin@swansea.ac.uk

Keywords: graphene, pH Sensor, melanin, screen print, blood plasma, low cost manufacturing

Supplementary material for this article is available online

Abstract

The application of highly sensitive pH sensors manufactured in volume at low cost has great commercial interest due to an extensive array of potential applications. Such areas include industrial processing, biotechnology and medical diagnostics particularly in the development of point of care (POC) devices. A novel printable electrochemical pH sensor based on graphene and pigment melanin (PGM), was designed and produced by using a screen printing process that enables up scaling for potential commercial application. We demonstrate a highly sensitive pH sensor (62 mV $pH^{-1} \pm 7$) over a pH range from 5 to 8, with high stability and superior performance when compared with a number of existing devices and making it suitable for physiological applications.

1. Introduction

The measurement of the pH of a solution is of universal importance and is used extensively across a range of disciplines (e.g. chemistry, biology, environmental science), both in the laboratory as well as in the field [1–5]. As such, multiple techniques have been developed to measure the pH [6]. The most common applications for pH determination are based on potentiometry, usually using a glass electrode [7, 8]. Film electrodes and ion selective membranes are also used to measure pH potentiometrically as are ion selective field effect transistors [9, 10]. pH may also be measured using a variety of ductometric [11] and optical [12] methods including measuring colour changes in pH sensitive indicator dyes. This wide variety of ways to measure the pH is indicative of its universal importance i.e. its presence as a variable in many different kinds of systems.

However, there are drawbacks to the various approaches. Many of these methods are subject to sensors with a limited lifetime or their sensing time does not comply with the speed at which the pH of a system is changing, or the active material of a pH sensor is easily contaminated or the loss/degradation of the sensing substances occurs [13]. The ubiquitous glass electrode, as an example, is fragile and requires time to build up a hydrate layer before usage. Furthermore, the ability to optimise it is challenging since remodelling options are limited [13].

As a result, there is a continuing active interest in finding new methods for measuring pH. Recent studies show many material options (organic and inorganic) that can be used as ion sensitive layers (see table 1 for examples). Ideally, a pH sensor needs to have the following properties if it is to be used widely:

1. Easy to produce in a commercial setting.
2. Made of readily available materials.
3. Be sensitive, i.e. a high electrochemical voltage versus pH gradient across a wide pH range. Failing that across a specified, widely studied pH range.
4. That the sensor is stable over the pH range as well as over time (little degradation).
5. Ideally fast response time.

The purpose of this paper is to demonstrate a commercially viable, robust and sensitive pH sensor that rivals that of 3D graphene with HfO_2 & IrO_2/RGO (table 1) but utilising readily available materials.

1.1. Screen printing

One of the ways to achieve low cost manufacturing to produce in a commercial setting is via a screen-printing process. The added benefit of this process is that it opens new avenues for other kinds of sensors.

Screen-printing is an attractive technique for the production of sensors, because the technology is well established and allows for rapid production. Screen printing is often used for the fabrication of electrodes due to the low cost and simplicity of the technique [28, 29].

Furthermore, the base electrode material of interest for this application is based on carbon, since it has been studied extensively and is often used in electrochemistry due to its electrical conductive properties, low density and low thermal expansion [30]. Specifically, we target graphene as the main electrode due to its reported use as an electronic material [31], sensor in bioelectronics [32, 33] and in applications based on its high carrier mobility and high carrier concentration. Also it has, biocompatibility, atomic thickness, electrochemical stability and mechanical reliability [34].

However, as will be shown below, graphene on its own is not sensitive enough in this specific application. Instead, this study explores the possibility of using a melanin derivative as the pH sensitive medium in combination with a printed graphene (PG) working electrode. The graphene electrode has been chosen due to it good electrical conductivity and the ability to control its printed topography on which melanin is spin coated to form a very thin layer.

1.2. D-melanin

The melanins are a class of conjugated biomacromolecule [35]. The most common form, eumelanin, is considered the archetypal melanin [35] and forms the basis of our discussion for the rest of the manuscript. As such, we will follow standard literature nomenclature and refer to it as 'melanin'. In nature, melanin has many biological functions and properties including photoprotection [35–37], neuroprotection [38], free radical scavenging [39] and structural colouration [40]. They are commonly present in biological systems and they can also be produced synthetically [35, 40]. Both naturally occurring and synthetic melanins have recently been receiving attention as versatile biomolecules with the potential for various biomedical applications [41]. The structure of melanin is believed to be composed of macromolecules of 5,6-dihydroxyindol-quinone (DHI) and 5,6-dihydroxyindole-2-carboxylic acid (DHICA) as can be seen in (figure 1). Indeed, melanin is a unique physio-chemical system with properties including hydrophilicity [42, 43], hydration dependent conductivity [44–47], free radical properties [48–51], metal ion chelation [52] and a broad band UV–Vis absorbance [53, 54]. As a result melanin has been studied for applications in UV filters [55], solid-state organic electrochemical transistors [56], metal-insulator devices [57], flexible supercapacitors [58], extended gate field effect transistors (EGFETs) for pH sensing [27], engineered electrodes [59] and edible batteries [60].

Table 1. Examples of different sensing materials used as active components in pH sensors.

Sensor material	Sensitivity (mV pH^{-1})	Range (pH)	Ref.
IrO_2	−51.1	1.5–12	[14]
(SM_2O_3)	56.2	2–12	[15]
C/PANI	50	4–10	[16]
RuO_2/SnO_2	56.5	2–12	[17]
GO	31.8	4–10	[18]
IrO_2/RGO	62	2–12	[19]
3D—G with HfO_2	71 ± 7	3–9	[20]
RGO	40 ± 5	4–10	[21]
SnO_2	56–58	2–12	[22]
ZnO	38	2–12	[23]
ITO	55	1–11	[24]
PANI/PVSA	58	2–12	[25]
CNT	50.9	3–13	[26]
Melanin/ITO/Au	48.9	2–12	[27]
PGM	62 ± 7	5–8	This work

G: graphene, CNTs: carbon nanotubes, GO: graphene oxide, RGO: graphene oxide, IrO_2: iridium oxide, SM_2O_3: samarium oxide, RuO_2/SnO_2: ruthenium oxide/tin oxide, PANI/PVSA: polyaniline/poly vinyl sulfonic acid, ZnO: zinc oxide, ITO: indium tin oxide, Au: gold, HfO_2: hafnium oxide.

What makes melanin particularly attractive as an active electrochemical sensing material is its reported sensitivity as a function of pH (~ −50 mV pH^{-1}) [27, 61]. The electrochemistry is due to the hydroxyl groups of quinone moieties and the interconversion between the various oxidative states [46, 47] (figure 2). Furthermore, melanin films have been used previously as an active layer in a pH sensing EGFET producing a higher sensitivity to pH than indium tin oxide [27]. Additionally, the material is cheap to synthesise and is very robust. However, it has one flaw, it is partially soluble at moderate to high pH.

As a consequence, we turn to a melanin derivative referred to as DMSO melanin (figure 3). DMSO melanin or D-melanin, is melanin that is synthesised in DMSO instead of water, the standard solvent [64, 65]. This material has several advantages over standard melanin. These include ease of spin coating of both hydrophobic and hydrophilic surfaces and stability in aqueous solutions of differing pH, including alkaline solutions [66]. The former property means that DMSO melanin can be spin coated on substrates which require minimal preparation and the latter property makes it very attractive for pH sensing.

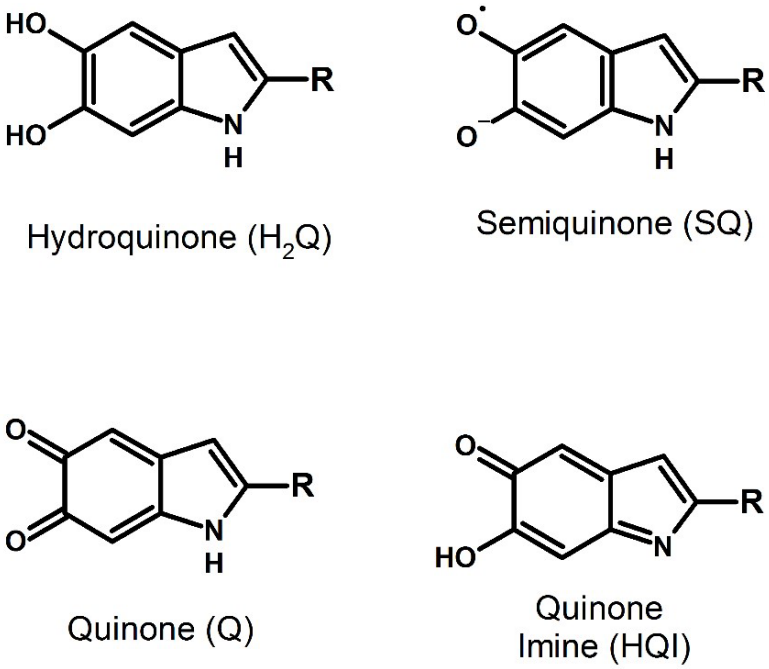

Figure 1. Eumelanin, the brown-black pigment, is synthesised initially from the hydroquinone monomer, 5,6-dihydroxyindole (DHI, i.e. R = H) and 5,6-dihydroxyindole-2-carboxylic acid (DHICA, i.e. R = COOH) [35]. The various differing oxidative states for the monomer are also given, since as melanin is formed under oxidative conditions, these other monomers also become incorporated into the polymer.

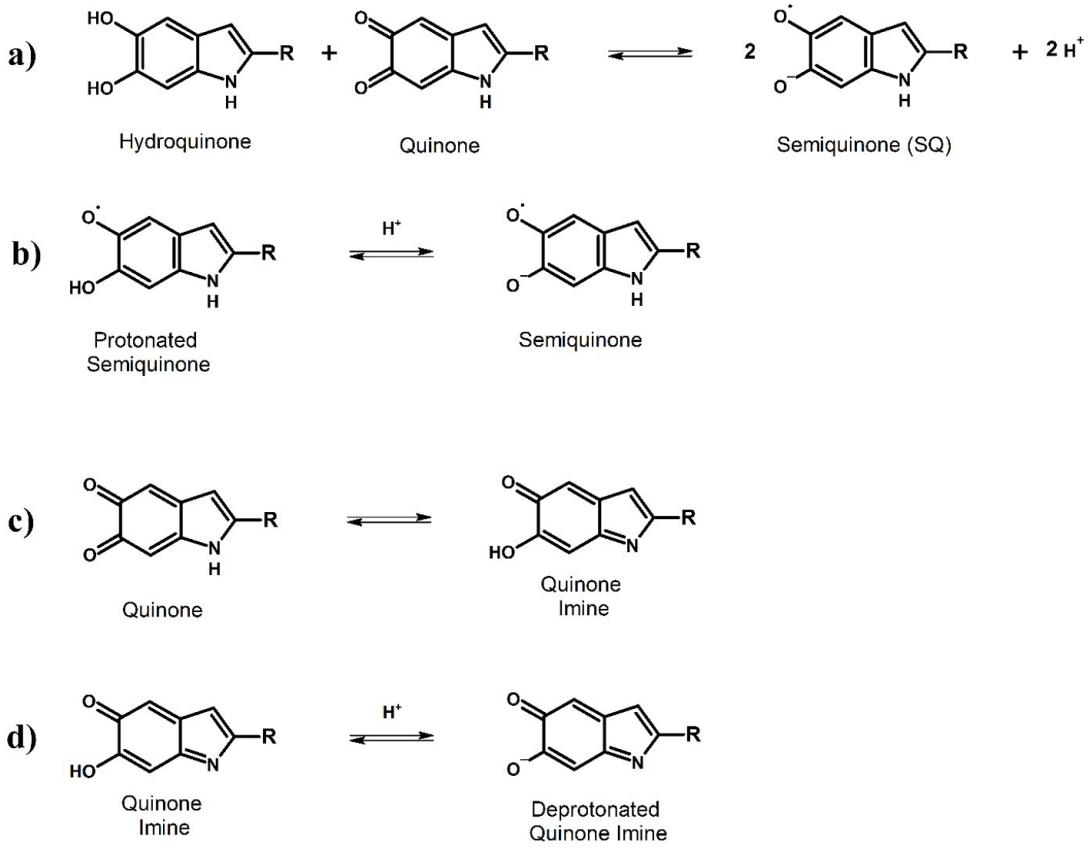

Figure 2. (a) The comproportionation reaction. Moieties of two differing oxidative states (hydroquinone and quinone) react together with water to form an intermediate oxidative state (the semiquinone) and hydronium [62] (b) the (de)protonation of the semiquinone. (c) Melanin is an unusual quinone system in that its quinones can undergo tautomerization to the quinone imine [63] (d) the final reaction is the (de)protonation of the quinone imine.

2. Materials and fabrication

2.1. Materials for screen printing

Polyethylene terephthalate (PET) with a thickness of 175μm (HIFI Melinex 339) was used as the substrate. This film is heat stabilized to provide high temperature resistance and hence dimensional stability during processing [68]. This was used as is.

Screen printed electrodes were prepared by first printing conductive silver (SunTronic ref: AST6025) or silver/silver chloride (Gwent ref: C2130809D5). This highly conductive silver polymer ink was selected for the printable refence electrode. It has been developed for a wide range of electronic applications [69] and has the following characteristics necessary for this application: compatibility with carbon inks, high stability and long-term storage, excellent adhesion to PET substrates after sintering. Carbon and graphene ink mixture (Gwent ref: C2171023D1) were used as a working electrode and finally a layer of insulating ink (Gwent ref: D214011D5) to protect the electrode.

2.2. Synthesis of melanin

Melanin was synthesized from 3,4-dihydroxyphenyl-DL-alanine (DL-Dopa; Sigma-Aldrich, ⩾98%) with dimethyl sulfoxide (DMSO; PA, Vetec, 99.9%) following a literature procedure [67]. 1.50 g of DL-Dopa and 0.93 g of benzoyl peroxide (Vetec, 75.0%–80.0%) were dissolved in 200 ml of DMSO and kept under magnetic stirring for 58 d at room temperature (≈27 °C.). Afterwards, the reaction solution was concentrated to 1/4 of the initial volume by increasing the temperature to 140 °C. Once it cooled down to room temperature, 150 ml of acetonitrile (Synth, 99.5%) was added to the concentrated solution to allow the melanin to be separated from synthetic by-products. After two days, the solution was centrifuged at 2500 rpm for 15 min and the precipitate dried in an oven at 90 °C. The black/dark brown powder obtained was used to make a 30 mg ml^{-1} solution for film fabrication.

2.3. pH-sensor fabrication

2.3.1. Fabrication of electrodes by screen-printing

The components of the sensor were printed using a R29 series screen printer from Reprint (UK) under ambient air conditions. Basically, during the screen-printing process, the ink is applied on the substrate through a screen imaged according to the sensor layer requirements. The substrate was cleaned using isopropyl alcohol (IPA) before printing the bottom and top electrodes of the sensor in a stack configuration. The printing of electrode comprises four steps that include silver/silver chloride printed as a reference electrode, carbon printed as a current electrode and graphene as a working electrode, thin film melanin covered the graphene layer and finally some parts of the electrode were covered with an insulator ink. The design of the PGM sensor is shown in figure 4.

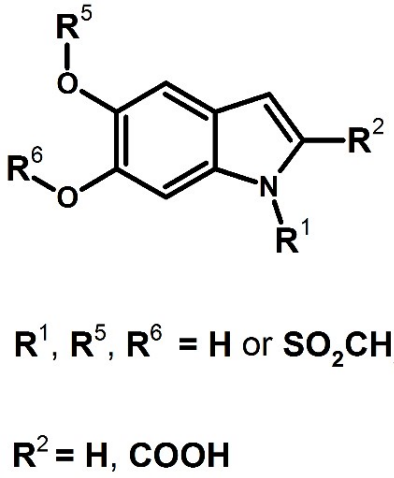

Figure 3. Basic monomeric moieties proposed for DMSO melanin [67]. In addition to the standard moieties indicated in figure 1, many moieties are believed to form methylated sulfonate groups at the reactive sites of the initial starting monomer with various degrees of methylation.

There are many process settings that can influence the printed layer, deposition thickness, uniformity and topography, where final parameters settings are summarised below.

The different parameters are the following: 50 mm · s^{-1} forward speed, 10 mm · s^{-1} reverse speed, 5.0 front squeegee pressure, 2.0 mm print gap and no snap-off distance (0.3 mm · s^{-1} snap speed) figure 1S in supplementary information (SI) (stacks.iop.org/TDM/7/024008/mmedia) for details of printing. Through a comprehensive experimental programme, this was optimised to achieve print to print consistency, thus assuring a path to full scale manufacturing. When these were established, they were found to deposit layers having consistent thickness and appropriate topography. Screens made of polyester having appropriate thread count and thickness for each ink layer were used and the associated oven temperature for the drying regime is summarised in table 2.

For the final step, 30 mg of DMSO melanin was dissolved in 1 ml of anhydrous DMSO (Sigma-Aldrich, ⩾99.9%) which was stirred for 1 hour at 50 °C and then filtered with a 0.45 μm Hydrophobic PTFE filter (Cole-Parmer). This solution was then spin coated using two steps: first step, at 1000 rpm for 60s; and the second step at 4000 rpm for 30s to form the final PGM.

Thus, a very thin film of melanin was deposited on the screen-printed graphene electrode (PGM) by spin coating and the sensor was ready for testing.

2.4. Characterisation techniques

The layers that formed the electrodes was characterized for their thickness and topography using different

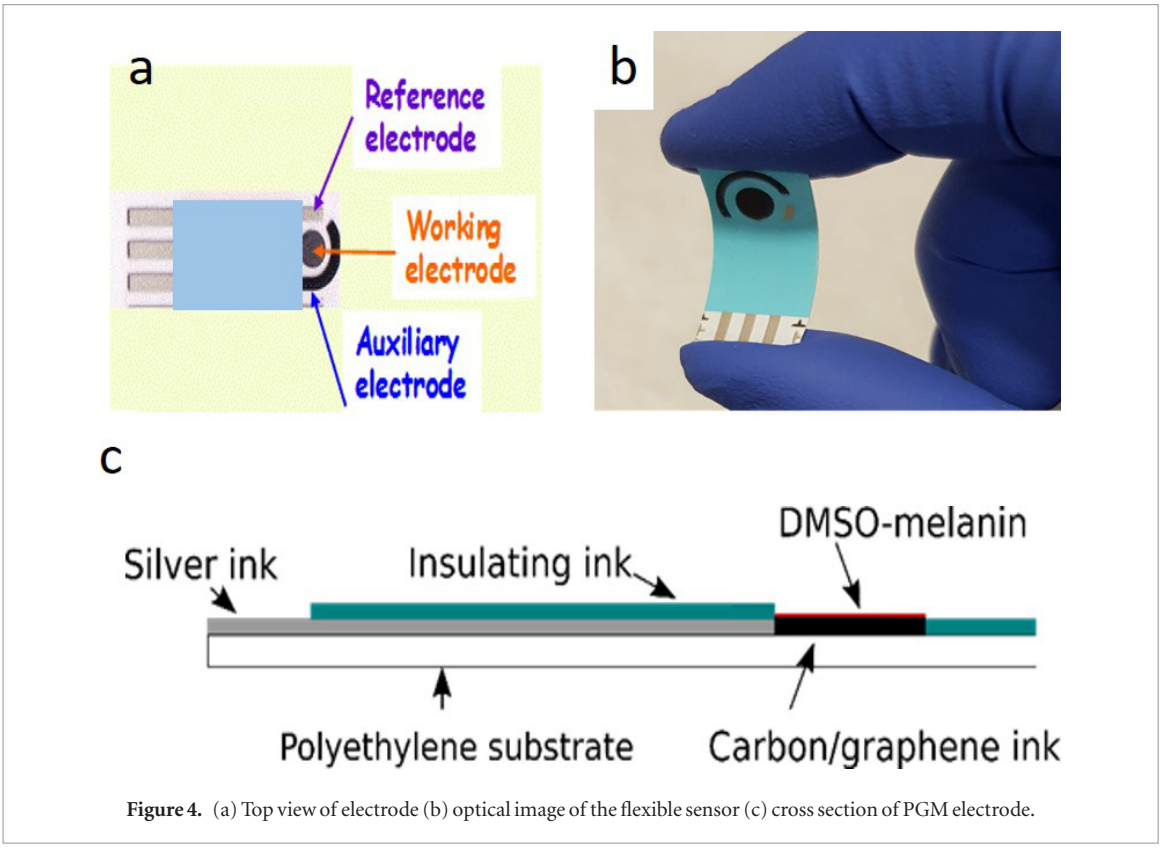

Figure 4. (a) Top view of electrode (b) optical image of the flexible sensor (c) cross section of PGM electrode.

Table 2. Summary of printing and drying settings.

Ink	Screen used-polyester	Drying regime in oven
Silver	120–43	15 min @ 100 °C–110 °C
Carbon	61–64	15 min @ 100 °C–110 °C
Graphene/carbon	61–64	10 min @ 90 °C–100 °C
Insulator	61–64	25 min @ 100 °C

techniques to check the quality of the printed layers. These techniques include atomic force microscopy (AFM), white light interferometry (WLI) and scanning electron microscopy (SEM). These were applied at the different stages of fabrication.

AFM was carried out using a JPK NanoWizards II. (Dimension-3100 Multimode, Bruker, Billerica, MA, USA), using a non-contact AFM tip with resonant frequency, spring constant and tip radius of 320 kHz, 40 N m^{-1} and 8 nm respectively operated on AC mode.

WLI was performed using a Veeco Wyke NT9300 optical profiling system.

Scanning electron microscopy (SEM; Ultra-High-Resolution FE-SEM S-4800, Hitachi) was carried out at 2.5 kV acceleration voltage and a 9.8 mA emission current. The magnification was ×20 k and working distance was 10.8 mm.

X-ray photoelectron spectroscopy (XPS) measurements were taken with a Kratos Axis Supra XPS system with a monochromatic Al Kα x-ray source, with an emission current of 15 mA.

The Fourier-transform infrared (FTIR) measurements were obtained between 4000 and 400 cm^{-1}, at room temperature, this technique has been employed to analyse D-Melanin in the sensor (SI figures 3S and 4S).

Raman mapping measurements were taken with an Renishaw system utilising a 532 nm excitation laser with approximately 10mW of power on the sample, before and after melanin deposition (SI figure 5S).

Electrochemical analysis was performed using the advanced potentiostat (PGSTAT-302 from Autolab, Metrohm Autolab, Runcorn, UK) with the scanning voltage in the range of 0.0 V–0.8 V for evaluating the electrochemical performance of PG and PGM electrodes. The standard 3-electrode system was used for the electrochemical evaluation, where printed graphene/melanin was used as the working electrode, Ag/AgCl as the reference electrode and printed carbon as the counter electrode. 5 mM $K_3[Fe(CN)_6]$/$K_4[Fe(CN)_6]$ in solution phosphate buffer saline (PBS) solution (pH = 7.4) was used as an electrolyte. To check the consistency of the sensor, four different samples were tested (SI figures 6S and 7S).

To test pH measurement, sensors were connected to the Ana-Pot from Zimmer and Peacock ltd set at a current range of 100 nA and measured for 600s in different buffer solutions (SI figure 9S).

Electrical measurements were performed using a 4-probe 'EverBeing probe station' with a 2636B Keithley Unit.

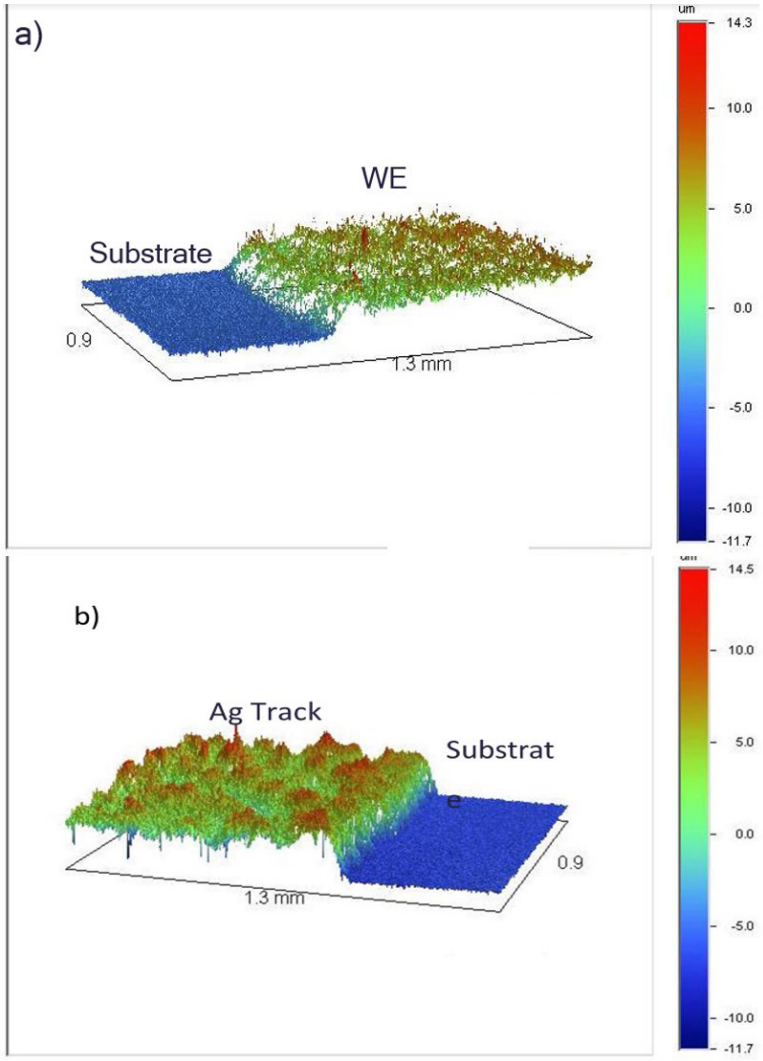

Figure 5. An example of an axonometric profile of the surface using WLI. (a) Carbon–graphene electrode (b) Ag track.

Table 3. Summary of thickness of different layers.

Layer	Thickness(μm)	Roughness(μm)
Ag/AgCl	10.63 ± 0.8	0.42 ± 0.19
Ag/AgCl110GPH	11.33	—
PG	8.61 ± 0.9	1.24 ± 0.12
G-110GPH	10.625	2.15
Insulator	14.5 ± 1.09	0.41 ± 0.05
PGM	0.268 ± 0.03	282.66 ± 0.019

G: grapheme.

3. Results and discussion

3.1. Characterization of graphene-melanin electrode: surface morphology

The layers that formed the electrodes fabricated using screen printing was characterized for their thickness and topography.

WLI was used to measure the thickness and roughness of different parts of the sensors (figure 5).

As a benchmark, a comparison of thickness and roughness between the in house printed graphene/carbon (PG) electrode with a commercial screen-printed electrode (Metrohm Drop Sense DRP-110GPH) is shown in at table 3. Five measurements were taken at three rows and three columns in three different sheets of printing resulting in a total of 90 measurements collected (for each layer: silver and graphene) the results are shown in at table 3. Where the standard deviation is noted to be very small, thus confirming dimensional consistency (SI figure 16S).

The roughness of the commercial sensor electrode (2.1 μm) is rougher than the PG (1.2 μm see table 3). However, the PG sensor has a more uniform roughness and the smoother surface is advantageous for the complete coverage of the electrode by a very thin melanin layer (figures 12S–14S)

The SEM images show the uncoated printed graphene (PG) and the melanin coated graphene (PGM). The small particles (carbon black) and the flake like materials are present in both of the images taken before and after melanin coating took place. This is expected as the melanin molecules are extremely small and therefore not detectable by our SEM. These images show the surface structural characteristics of the working electrode and how they appear to be unchanged

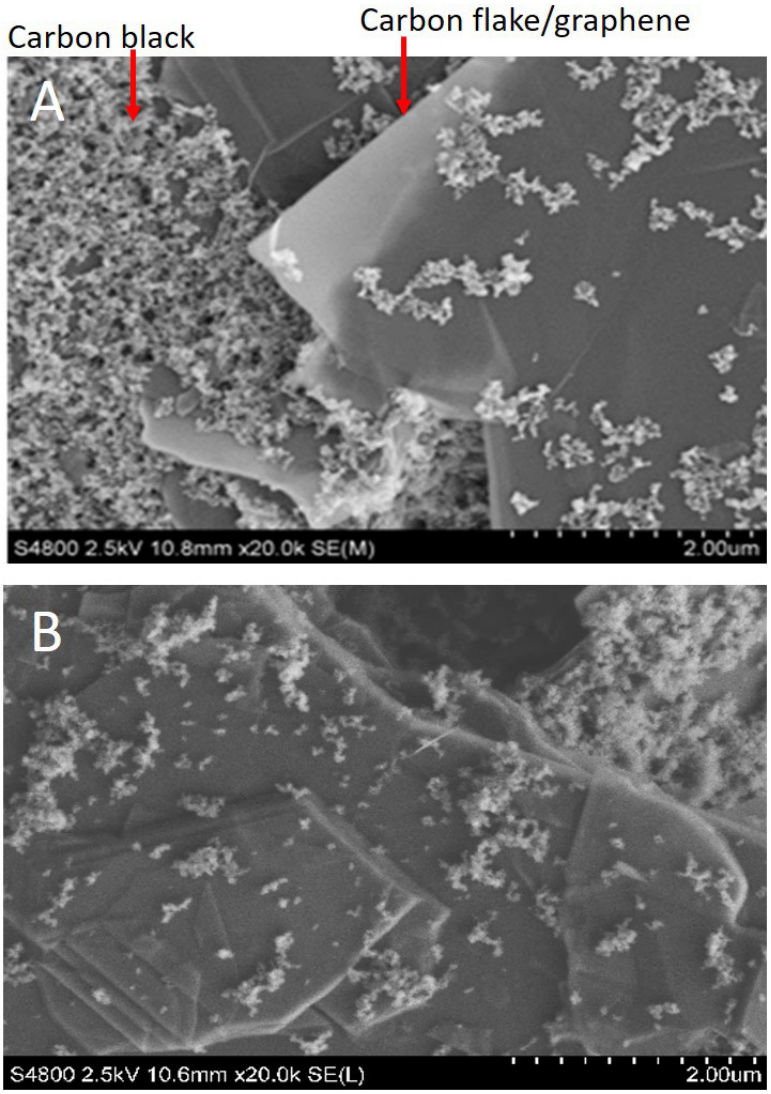

Figure 6. Morphology top view of electrode with SEM (a) before coating- PG (b) after coating the melanin (PGM).

visually at the SEM level following melanin coating. This shows that the amount of melanin that is required for the electrode to become functionalised and therefore sensitive to pH is extremely small (figure 6).

The effect of surface morphology of thin film of melanin was also explored using AFM, figure 7.

The surface roughness of PG substrates before and after melanin deposition (figure 7) shows clear changes in surface topography. The Root Mean Square roughness of 102.1 nm before deposition (figure 7(a)) increases to 292.5nm after deposition (figure 7(b)).

3.2. Characterization of graphene-melanin electrode: surface chemistry

Raman mapping measurements were taken with a Renishaw inVia system using a 532nm laser, before and after melanin deposition. The ratio between the G-peak, at 1580 cm^{-1}, and the D-peak, at 1350 cm^{-1}, were mapped out using a custom MATLAB script (SI figure 4S).

As seen in (figure 8), the intensity of the D-peak is significantly higher, resulting in the D-peak/G-peak intensity ratio increase from 0.0744 to 0.0914. The D-peaks are most likely from the additional carbon compounds that are found in the carbon ink and from the application of melanin. The Raman system detects these additional carbon compounds, especially after melanin application, resulting in an increased signal in the D-band [70].

The intensity ratio between the 2D-peak and G-peak in monolayer graphene is approximately 2 [71]. However, this ratio decreases to approximately 0.398, in the printed graphene electrode, denoting that there are multiple layers of graphene present on the electrode [72].

We obtained high-resolution XPS measurements for N1s spectra as a reference for the chemical composition of the blank surface (figure 9, red curve). We then did a comparison test by obtaining data for d-melanin alone and then a melanin-coated electrode. In figure 9, it can be seen that melanin has only one broad nitrogen-peak ranging from 397 to 403 eV related to amine groups in its aromatic structure (figure 1), in agreement with previous studies [67] while the graphene

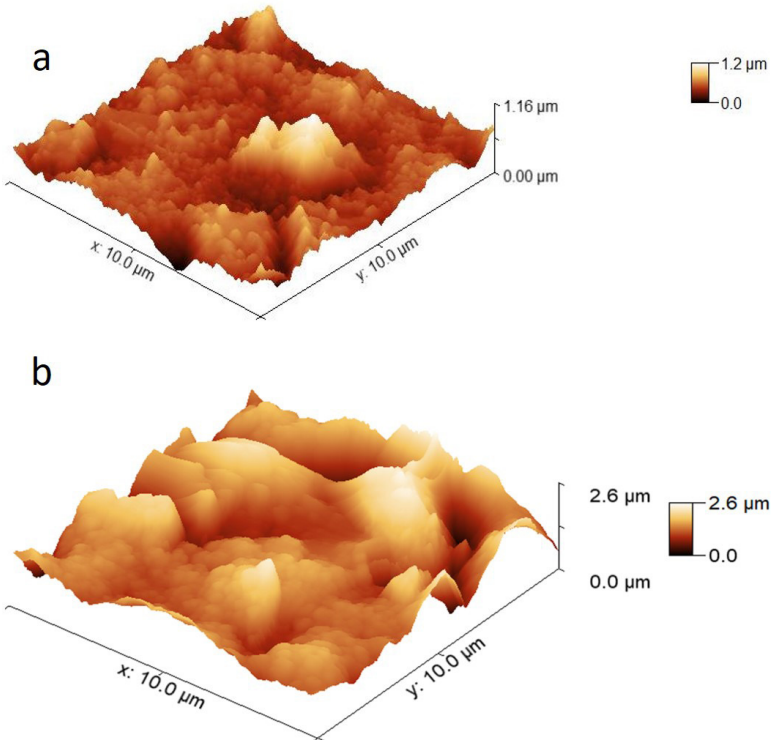

Figure 7. Morphology of electrode with AFM (a) before coating- PG (b) after coating the melanin (PGM).

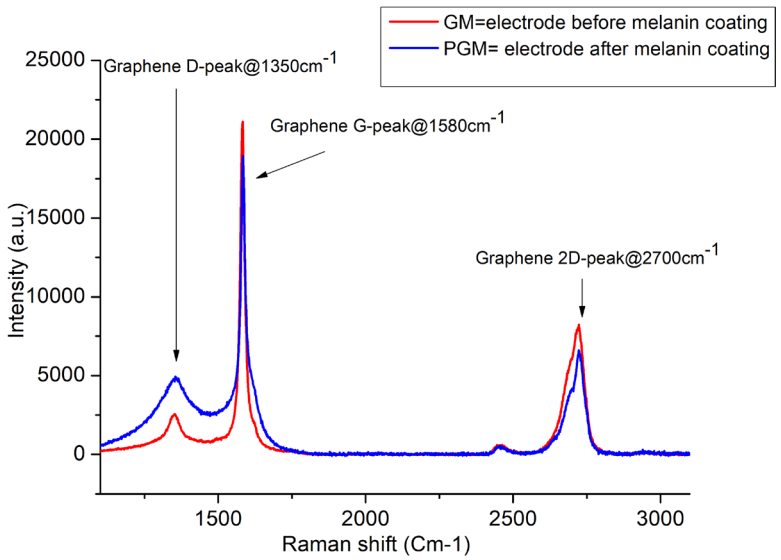

Figure 8. (a) Raman spectra of the electrode before (red) and after melanin coating (blue).

ink also has only one nitrogen peak at 408.2 eV from nitrate compounds. When the graphene electrode is coated with a melanin layer however, both nitrogen peaks can be observed. This indicates the presence of the melanin on the graphene. The small shift towards lower binding energies found for the peak at 408 eV, when melanin is present, is probably related to structural and/or electronic interaction between melanin and graphene [73]. (SI for atomic concentration of carbon and both nitrogen components in table 1S).

We performed Square Wave Voltammetry (figure 10) to characterise the electrochemistry of the electrodes. In this type of curve, the potential of the working electrode can be found with the maximum/peak of the curve. As can be seen, there is a clear difference between the electrochemical behaviour of just the bare electrode and afterwards when it is coated with D-melanin. There are shifts in current and voltage peaks, clearly showing that the D-melanin was deposited with good electrical contact, this test was carried out on multiple samples (table 4).

3.3. Four-point resistance measurements

IV curves using four probes revealed that there was a change in the resistance across the surface of the blank screen-printed electrode following melanin

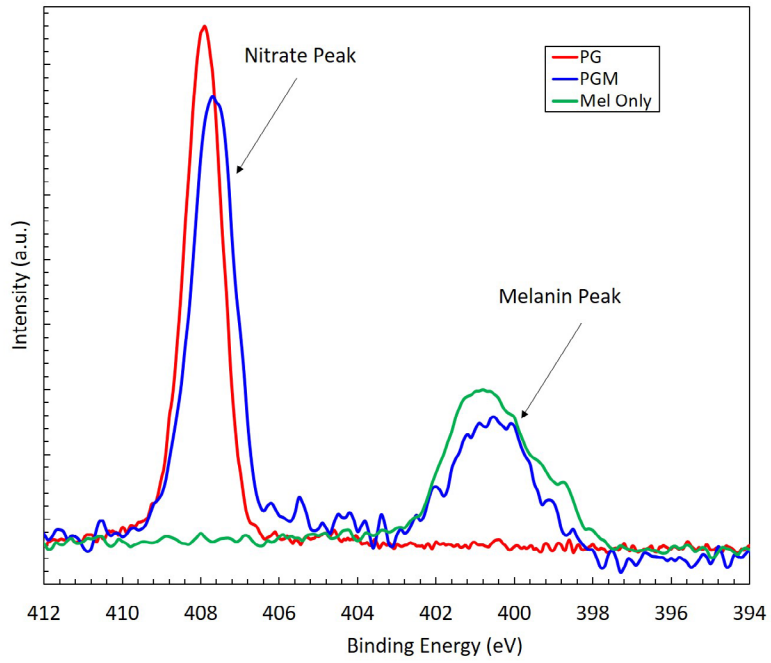

Figure 9. High-resolution N1s XPS spectra for melanin, graphene ink and melanin coated SPE. The presence of the nitrogen peak around 401 eV indicates that melanin is present at the surface of the sensor working electrode.

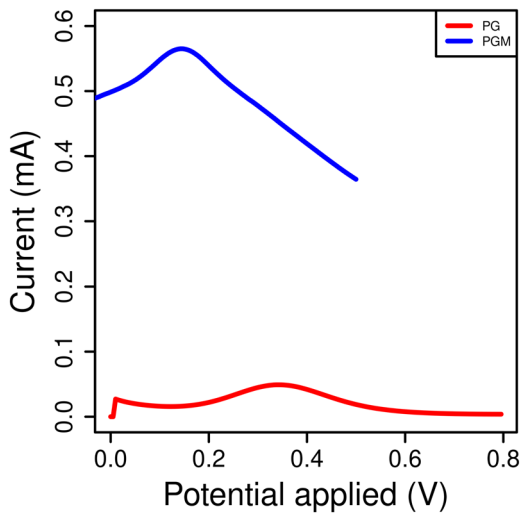

Figure 10. An example Square Wave Voltammogram showing the change in peak current and peak voltage: for PG (red) and PGM (with melanin) (blue).

deposition. Five blank PG and five PGM were tested. Each electrode was tested at five different positions on the electrode to account for any heterogeneity in film deposition. Five measurements were taken at each position resulting in a total of 250 data points collected (125 PG, 125 PGM) the results are shown in (figure 11). The data clearly indicates that the melanin is present by the way it modifies the resistance measured.

3.4. Potentiometric measurements

Having shown the characterisation of the electrodes, we now go on to demonstrate its sensing capabilities. The electrodes' potential (PG and PGM) was measured as a function of time in reference buffers

Table 4. Peak current and voltage of electrode at different layers.

Electrode	Peak current	Peak voltage
Blank	$0.05 \pm 0.000\,85$ mA	$0.34 \pm 0.003\,36$ V
PGM	$0.55 \pm 0.042\,21$ mA	$0.15 \pm 0.005\,81$ V

pH4, pH7 and pH10, to see stability of the device over time. The difference between the voltage recorded with each reference buffer is presented in (figure 12).

As can be seen, the PG electrode does not show any pH dependence at low pH. At high pH there is a dependence, but the electrode voltage decays over time. In contrast, the PGM (D-melanin coated) electrode shows a clear and significant change as a function of pH. In addition, and importantly, the potential is stable over time, showing a robust and instantaneous response to the pH.

3.5. Measured potential relationship to pH

The potential of the PGM electrodes were recorded continously in solution as the pH was changed (figure 13(a)) to demonstrate that the sensor can detect changes in the pH in real time. As can be seen, there are clear changes in the potential at every pH change. The sensitivity of the devices 35 ± 12 mV pH^{-1} over the pH range from 2 to 12 (SI figure 9S).

We did a further real time monitoring test by checking the hysterysis of the electrode behaviour. We did a test of the pH response going from pH 4 to 10 and then from 10 to 4 (figure 13(b)). As can be see, the potential measured at the given pH and shows little hysterysis.

The above test were done to demonstrate the sensitivity and robustness of the devices across a wide range of pH. However, we are particualrly interested in

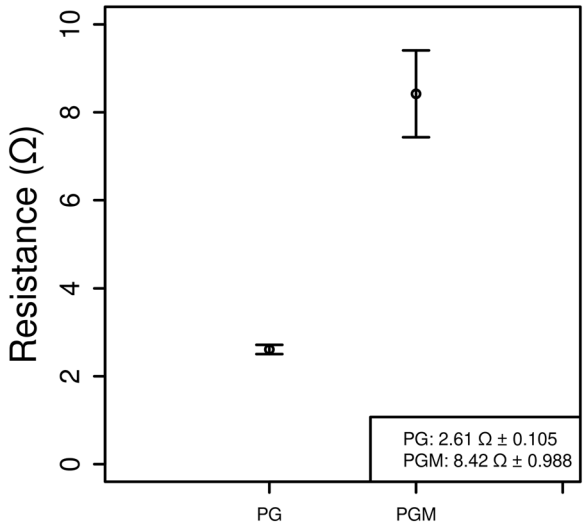

Figure 11. Average resistance measurements on melanin (PGM) on non-melanin (PG) coated electrodes, error bars represent the standard error multiplied by 2, with 125 data points for each condition.

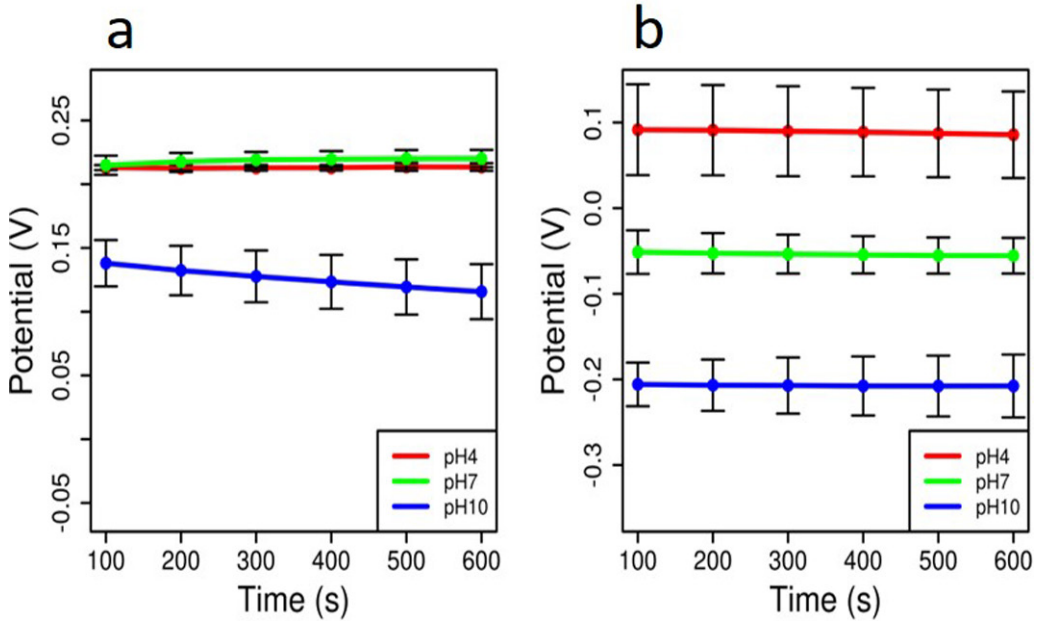

Figure 12. The potential difference of electrode in pH specific reference buffers with averages ($n = 3$). (a) PG: before deposition of melanin (b) PGM: after deposition of melanin to the electrode.

applying these devices for physiological measurements since there is a high demand for measurement of pH in medical settings. As such, we narrowed the range of pH to be studied to between pH 5 and 8.

The open circuit potential (OCP) is measured using the potentiostat. No voltage is applied. The voltage potential that is measured is the difference between the working electrode and the reference electrode, this difference changes based upon the pH of the solution that the sensor is immersed in. The counter electrode balances the charge on the working electrode.

We obtained a sensitivity curve across this range by selecting the pH with a reference buffer and then measuring the potential (figure 14(a)). The sensitivity value we obtained is 62 ± 7 mV pH^{-1} (table 5), an excellent result rivaling those of 3D graphene with HfO_2 & IrO_2/RGO [19, 20] (table 1).

The major advantage of our sensor, in contrast to the above mentioned sensors is that it was made from commonly avaiable materials coupled to a commerically viable low energy process for fabrication. We now move onto testing of the stability and repeatability of the PGM electrode at physiological pH values. Five PGM electrode were tested using a solution at pH 5 for 10 min followed by pH 5, pH 6, pH 7 and pH 8 solutions. As can be seen, a consistent change in the

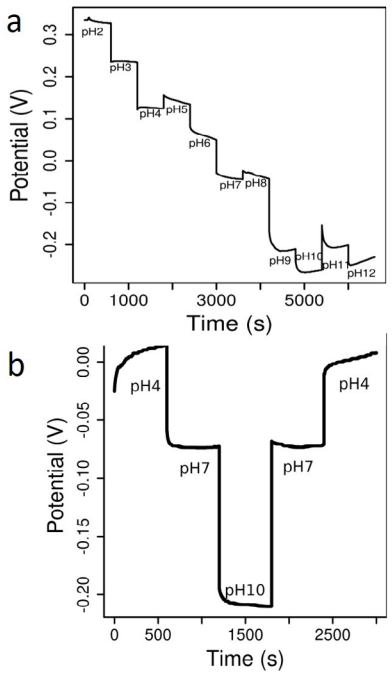

Figure 13. pH sensing performance of PGM (a) at extreme pH ranges 2–12, (b) the PGM electrode tested for its ability to recover following exposure to a high pH solution.

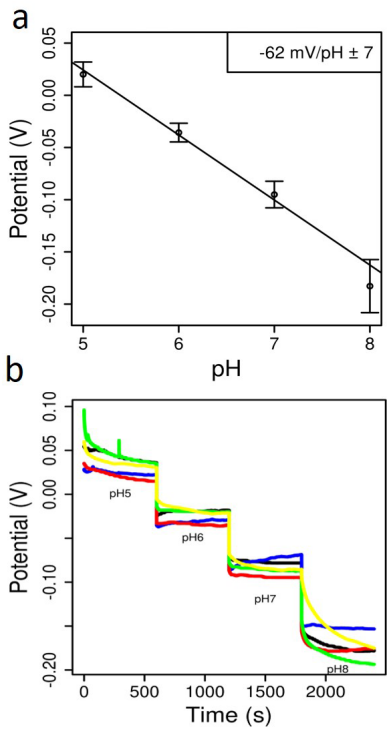

Figure 14. Sensing results and sensor characterization, (a) the slope was calculated using weighted least squares regression to an uncertainty of two times the standard error with each solution indicated that the sensor remains highly sensitive to pH changes following exposure to pH levels for physiological environment (b) stability and repeatability of the pH sensor. Data from the electrode was reanalysed using the standard error ×2 in order to produce the error bars.

measured potential was seen across all the replicates (figure 14(b)), indicating that there is consistency across the fabrication process.

3.6. Mechanism of action

We now turn to the potential mechanism of operation for the DMSO melanin pH sensor. The first thing to note is that the pH sensitivity that has been recorded is in line with previous pH/E data published on standard melanin [27, 61]. This initial observation is surprising at first, since one would expect a difference between standard melanin and DMSO melanin which contains additional sulfonated moieties (figure 3). However, the pH/E behaviour is most likely due to the reduction potentials of the one electron redox reactions for the quinone/semiquinone and semiquinone/hydroquinone pairs [47]. Both these reactions together yield the comproportionation reaction (figure 2(a)). This contrasts with our previous suppositions that the pK_as of the various constituents are responsible for the effect [73]. Instead, both the the pK_as and the positions of the redox potentials is what drives the redox chemistry and ultimately making our device a sensitive pH sensor.

With the above, it is apparent that the DMSO melanin electrochemically acts as a standard melanin, i.e. the standard comproportionation reaction is active. Considering that not all moieties in DMSO melanin will be sulfonated, there will then still exist a melanin fraction to undergo the electrochemistry. In contrast, the sulfonated moieties may in turn only be spectators electrochemically. Overall, it appears that DMSO

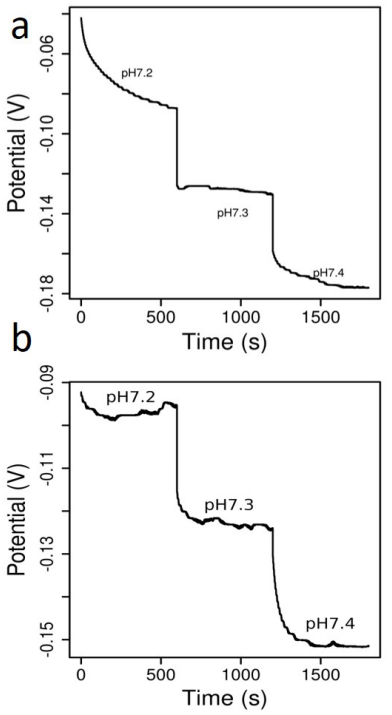

Figure 15. Potentials measured with pH7.2, pH7.3 and pH7.4 reference buffers for 10 min intervals (a) Fresh electrode (b) with the PGM sensors following testing with plasma.

Table 5. Sensitivity of the electrode at different pH range.

Stage	Sensitivity (mV pH^{-1})	pH range
Blank	12.65 ± 20	2–12
PGM -fresh	35 ± 12	2–12
PGM -reuse	33.8 ± 12	2–12
PGM -fresh	**62 ± 7**	5–8
PGM -reuse	60.24 ± 7	5–8

melanin has the same sensitivity as standard melanin due to similar redox chemistry, but with the additional advantages of material processibility and stability. The downside would be the presence of fewer standard melanin moieties. However, since the potential is what matters and not the total current, this is not a great problem and further device engineering should enhance the accuracy.

3.7. Preliminary tests with clinical samples.

Since we are particulary interested in applying these sensors in physiological conditions, we have performed preliminary tests of the sensors on blood plasma samples obtained from healthy volunteers since plasma is commonly used as a clinical sample type. To test the sensors, plasma was pipetted onto the surface of the sensor and the OCP was measured over a 10 minute period. Following exposure to plasma, the sensors were rinsed with distilled deionised water and measured with pH 7.2, pH 7.3 and pH 7.4 buffers (five PGM sensor were tested) to confirm their correct functioning (figure 15). The PGM sensor continued to exhibit sensitivity to the different pH buffers after being exposed to blood plasma, showing that the sensor is robust enough to be considered as a candidate in the development of applications where exposure to a clinical plasma sample is desired. This is an example curve for one of the five sensors that were tested (figure 14).

4. Conclusions

We have produced printed graphene electrodes with high reproducibility and good electrical conductivity using a novel screen printing process. The fabricated printed electronic sensor exhibited improved performance and properties when compared to a commercial sensor (DRP-110GPH) specifically with regards to reproducibility and homogeneity.

Furthermore, in using the active material DMSO melanin, a derivative of the pigment melanin (PGM), and which lends itself to the low energy fabrication, we are able to create a sensitive pH sensor. The sensor itself demonstrates high levels of both accuracy and precision within the physiologically relevant pH levels between pH 5 through to pH 8 (62 ± 7 mV pH^{-1}).

The above research provides the foundation for the later development and optimisation of the pH sensitive properties of the electrode to further increase its accuracy and sensitivity.

This suggests that the sensor will be well suited for applications that involve biological application and may also have potential applications within a clinical setting. The sensor is sensitive enough to detect clinically relevant changes in blood plasma pH which the preliminary test started.

In conclusion, a novel and highly sensitive pH sensor is demonstrated based on printed graphene coated with a thin film of melanin derivative, DMSO melanin. In short, we have produced a pH sensor that has the 'best of both worlds': low cost and reliable (i.e. commercially viable) while being very sensitive.

Acknowledgments

This research was funded by Knowledge Economy Skills Scholarships (KESS). ZT acknowledges the joint financial support from Welsh Government and European Commission under European Regional Development Funds (ERDF) through Sêr Cymru II Fellowships (Project Number: 80761-su-100). ABM is a Sêr Cymru II fellow and the results in this work have received funding from the European Union's Horizon 2020 research and innovation program under the Marie Sklodowska-Curie grant agreement no 663830. JVP and CFOG would also like thank the financial support of São Paulo Research Foundation (FAPESP; grants 2015/23000-1, 2018/02411-1). The authors wish to thank to Ms Zelia Lagors and Mr Hugo Spieser from Grenoble INP-Pagora France.

The authors would also like to acknowledge Dr Martin Peacock from Zimmer and Peacock Ltd.

The authors declare no conflicts of interest.

ORCID iDs

Z Tehrani https://orcid.org/0000-0002-5069-7921
A B Mostert https://orcid.org/0000-0002-9590-2124
C F O Graeff https://orcid.org/0000-0003-0162-8273

References

[1] Abdel-Rahman M A, Tashiro Y and Sonomoto K 2013 Recent advances in lactic acid production by microbial fermentation processes *Biotechnol. Adv.* **31** 877–902
[2] Guinovart T *et al* 2014 Bandage-based wearable potentiometric sensor for monitoring wound pH *Electroanalysis* **26** 1345–53
[3] Lemos S G *et al* 2007 Soil calcium and pH monitoring sensor system *J. Agric. Food Chem.* **55** 4658–63
[4] Phulara S C *et al* 2019 Modulation of culture medium confers high-specificity production of isopentenol in Bacillus subtilis *J. Biosci. Bioeng.* **127** 458–64
[5] Yang J *et al* 2016 Digital pH test strips for in-field pH monitoring using iridium oxide-reduced graphene oxide hybrid thin films *ACS Sensors* **1** 1235–43
[6] Yuqing M, Jianrong C and Keming F 2005 New technology for the detection of pH *J. Biochem. Biophys. Methods* **63** 1–9
[7] Baucke F 1985 The glass electrode—applied electrochemistry of glass surfaces *J. Non-Cryst. Solids* **73** 215–31

[8] Palleschi G *et al* 1994 Bioelectrochemical determination of lactic and malic acids in wine *Talanta* **41** 917–23
[9] Janata J 1990 Potentiometric microsensors *Chem. Rev.* **90** 691–703
[10] Komaba S *et al* 1997 Potentiometric biosensor for urea based on electropolymerized electroinactive polypyrrole *Electrochim. Acta* **42** 383–8
[11] Contractor A *et al* 1994 Conducting polymer-based biosensors *Electrochim. Acta* **39** 1321–4
[12] Ben-David O *et al* 1997 Simple absorption optical fiber pH sensor based on doped sol-gel cladding material *Chem. Mater.* **9** 2255–7
[13] Li J-P, Peng T-Z and Fang C 2002 Screen-printable sol–gel ceramic carbon composite pH sensor with a receptor zeolite *Anal. Chim. Acta* **455** 53–60
[14] Huang W-D *et al* 2011 A flexible pH sensor based on the iridium oxide sensing film *Sensors Actuators* A **169** 1–11
[15] Wu M-H *et al* 2009 Structural properties and sensing performance of high-*k* Sm_2O_3 membrane-based electrolyte–insulator–semiconductor for pH and urea detection *Sensors Actuators* B **138** 221–7
[16] Rahimi R *et al* 2016 A low-cost flexible pH sensor array for wound assessment *Sensors Actuators* B **229** 609–17
[17] Manjakkal L *et al* 2015 Sensing mechanism of RuO_2–SnO_2 thick film pH sensors studied by potentiometric method and electrochemical impedance spectroscopy *J. Electroanal. Chem.* **759** 82–90
[18] Melai B *et al* 2016 A graphene oxide pH sensor for wound monitoring *2016 38th Annual Int. Conf. of the IEEE Engineering in Medicine and Biology Society* (IEEE)
[19] Yang J *et al* 2016 Iridium oxide-reduced graphene oxide nanohybrid thin film modified screen-printed electrodes as disposable electrochemical paper microfluidic pH sensors *J. Vis. Exp.* **2016** e53339
[20] Ameri S K, Singh P K and Sonkusale S R 2016 Three dimensional graphene transistor for ultra-sensitive pH sensing directly in biological media *Anal. Chim. Acta* **934** 212–17
[21] Salvo P *et al* 2017 Temperature and pH sensors based on graphenic materials *Biosens. Bioelectron.* **91** 870–7
[22] Chi L-L *et al* 2000 Study on extended gate field effect transistor with tin oxide sensing membrane *Mater. Chem. Phys.* **63** 19–23
[23] Batista P and Mulato M 2005 ZnO extended-gate field-effect transistors as p H sensors *Appl. Phys. Lett.* **87** 143508
[24] Chou J-C, Chiang J-L and Wu C-L 2005 pH and procaine sensing characteristics of extended-gate field-effect transistor based on indium tin oxide glass *Japan. J. Appl. Phys.* **44** 4838
[25] Vieira N C *et al* 2011 Nanostructured polyaniline thin films as pH sensing membranes in FET-based devices *Sensors Actuators* B **160** 312–7
[26] Chien Y-S *et al* 2012 A novel pH sensor of extended-gate field-effect transistors with laser-irradiated carbon-nanotube network *IEEE Electron. Device Lett.* **33** 1622–4
[27] da Silva M P *et al* 2014 Melanin as an active layer in biosensors *AIP Adv.* **4** 037120
[28] Hart J P and Wring S A 1997 Recent developments in the design and application of screen-printed electrochemical sensors for biomedical, environmental and industrial analyses *TRAC Trends Anal. Chem.* **16** 89–103
[29] Cui G *et al* 2000 A disposable amperometric sensor screen printed on a nitrocellulose strip: a glucose biosensor employing lead oxide as an interference-removing agent *Anal. Chem.* **72** 1925–9
[30] Kahlert H 2008 Functionalized carbon electrodes for pH determination *J. Solid State Electrochem.* **12** 1255–66
[31] Wu Y *et al* 2012 State-of-the-art graphene high-frequency electronics *Nano Lett.* **12** 3062–7
[32] Ameri S K, Singh P and Sonkusale S 2014 Utilization of graphene electrode in transparent microwell arrays for high throughput cell trapping and lysis *Biosens. Bioelectron.* **61** 625–30
[33] Tehrani Z *et al* 2014 Generic epitaxial graphene biosensors for ultrasensitive detection of cancer risk biomarker *2D Mater.* **1** 025004
[34] Geim A K 2009 Graphene: status and prospects *Science* **324** 1530–4
[35] Meredith P and Sarna T 2006 The physical and chemical properties of eumelanin *Pigm. Cell Res.* **19** 572–94
[36] Gray-Schopfer V, Wellbrock C and Marais R 2007 Melanoma biology and new targeted therapy *Nature* **445** 851–7
[37] Lin J Y and Fisher D E 2007 Melanocyte biology and skin pigmentation *Nature* **445** 843–50
[38] Zucca F A *et al* 2004 The neuromelanin of human substantia nigra: physiological and pathogenic aspects *Pigm. Cell Res.* **17** 610–7
[39] Panzella L *et al* 2013 Atypical structural and pi-electron features of a melanin polymer that lead to superior free-radical-scavenging properties *Angew., Commun.* **52** 12684–7
[40] d'Ischia M *et al* 2015 Melanins and melanogenesis: from pigment cells to human health and technological applications *Pigm. Cell Melanoma Res.* **28** 520–44
[41] Meredith P *et al* 2013 Electronic and optoelectronic materials and devices inspired by nature *Rep. Prog. Phys.* **76** 034501
[42] Mostert A B *et al* 2010 Gaseous adsorption in melanins: hydrophilic biomacromolecules with high electrical conductivities *Langmuir* **26** 412–6
[43] Clulow A J *et al* 2017 The structural impact of water sorption on device-quality melanin thin films *Soft Matter* **13** 3954–65
[44] Mostert A B *et al* 2012 Role of semiconductivity and ion transport in the electrical conduction of melanin *Proc. Natl Acad. Sci. USA* **109** 8943–7
[45] Wünsche J *et al* 2015 Protonic and electronic transport in hydrated thin films of the pigment eumelanin *Chem. Mater.* **27** 436–42
[46] Sheliakina M, Mostert A B and Meredith P 2018 Decoupling ionic and electronic currents in melanin *Adv. Funct. Mater.* **28** 1805514
[47] Motovilov K A *et al* 2019 Redox chemistry in the pigment eumelanin as a function of temperature using broadband dielectric spectroscopy *RSC Adv.* **9** 3857–67
[48] Mostert A B *et al* 2013 Hydration-controlled X-band EPR spectroscopy: a tool for unravelling the complexities of the solid-state free radical in eumelanin *J. Phys. Chem.* B **117** 4965–72
[49] Batagin-Neto A, Bronze-Uhle E S and Graeff C F O 2015 Electronic structure calculations of ESR parameters of melanin units *Phys. Chem. Chem. Phys.* **17** 7264–74
[50] Mostert A B *et al* 2018 The photoreactive free radical in eumelanin *Sci. Adv.* **4** eaaq1293
[51] Paulin J V, Batagin-Neto A and Graeff C F O 2019 Identification of common resonant lines in the EPR spectra of melanins *J. Phys. Chem.* B **123** 1248–55
[52] Hong L and Simon J D 2007 Current understanding of the binding sites, capacity, affinity, and biological significance of metals in melanin *J. Phys. Chem.* B **111** 7938–47
[53] Tran M L, Powell B J and Meredith P 2006 Chemical and structural disorder in eumelanins: a possible explanation for broadband absorbance *Biophys. J.* **90** 743–52
[54] Meredith P *et al* 2006 Towards structure–property–function relationships for eumelanin *Soft Matter* **2** 37–44
[55] Gallas J M 1987 Optical lens system incorporating melanin as an absorbing pigment for protection against electromagnetic radiation *US Patent* no. US5036115A
[56] Sheliakina M, Mostert A B and Meredith P 2018 An all-solid-state biocompatible ion-to-electron transducer for bioelectronics *Mater. Horiz.* **5** 256–63
[57] Ambrico M *et al* 2011 Melanin layer on silicon: an attractive structure for a possible exploitation in bio-polymer based metal-insulator-silicon devices *Adv. Mater.* **23** 3332
[58] Kumar P *et al* 2016 Melanin-based flexible supercapacitors *J. Mater. Chem.* C **4** 9516–25

[59] Kim Y J et al 2013 Biologically derived melanin electrodes in aqueous sodium-ion energy storage devices *Proc. Natl Acad. Sci. USA* **110** 20912–7
[60] Bettinger C J and Whitacre J F 2015 A water-activated, ingestible battery *US Patent* no. US20150118526A1
[61] Horak V and Weeks G 1993 Poly (5, 6-dihydroxyindole) melanin film electrode *Bioorganic Chem.* **21** 24–33
[62] Felix C et al 1978 Interactions of melanin with metal ions. Electron spin resonance evidence for chelate complexes of metal ions with free radicals *J. Am. Chem. Soc.* **100** 3922–6
[63] Szpoganicz B et al 2002 Metal binding by melanins: studies of colloidal dihydroxyindole-melanin, and its complexation by Cu(II) and Zn(II) ions *J. Inorg. Biochem.* **89** 45–53
[64] Dezidério S N et al 2004 Thin films of synthetic melanin *J. Non-Cryst. Solids* **338–40** 634–8
[65] Bronze-Uhle E S et al 2013 Synthesis and characterization of melanin in DMSO *J. Mol. Struct.* **1047** 102–8
[66] Albano L G S et al 2016 Novel insights on the physicochemical properties of eumelanins and their DMSO derivatives *Polym. Int.* **65** 1315–22
[67] Paulin J V et al 2018 Structural and optical properties of soluble melanin analogues with enhanced photoluminescence quantum efficiency *Polym. Int.* **67** 550–6
[68] HIFI Melinex 339 PET film (www.hififilm.com/product/melinex-339)
[69] Tehrani Z et al 2017 Large-area printed supercapacitor technology for low-cost domestic green energy storage *Energy* **118** 1313–21
[70] Taylor C E, Garvey S D and Pemberton J E 1996 Carbon contamination at silver surfaces: surface preparation procedures evaluated by Raman spectroscopy and x-ray photoelectron spectroscopy *Anal. Chem.* **68** 2401–8
[71] Ferrari A and Robertson J 2001 Resonant Raman spectroscopy of disordered, amorphous, and diamondlike carbon *Phys. Rev.* B **64** 075414
[72] Das A, Chakraborty B and Sood A 2008 Raman spectroscopy of graphene on different substrates and influence of defects *Bull. Mater. Sci.* **31** 579–84
[73] Gargiulo V et al 2015 Supplementing π-systems: eumelanin and graphene-like integration towards highly conductive materials for the mammalian cell culture bio-interface *J. Mater. Chem.* B **3** 5070–9